

TRIETHOXYSILYLPROPYLAMINE MODIFIED  
ALKALI TREATED WHEAT STRAW: AN EFFICIENT ADSORBENT FOR  
METHYL ORANGE ADSORPTION

HOOSHYAR MOGHIM ALIABADI,<sup>\*</sup> ELHAM SABERIKHAH,<sup>\*</sup>  
AZADEH EBRAHIMIAN PIRBAZARI,<sup>\*,\*\*</sup> REZA KHAKPOUR<sup>\*\*</sup> and HOUMAN ALIPOUR<sup>\*\*</sup>

<sup>\*</sup>*Fouman Faculty of Engineering, College of Engineering, University of Tehran,  
P.O. Box 43515-1155, Fouman 43516-66456, Iran*

<sup>\*\*</sup>*Caspian Faculty of Engineering, College of Engineering, University of Tehran, P.O. Box 43841-119,  
Rezvanshahr 43861-56387, Iran*

✉ *Corresponding author: H. M. Aliabadi, haliabadi@ut.ac.ir*

Received December 8, 2016

In this work, alkali treated wheat straw (ATWS) materials were simply modified by triethoxysilylpropylamine (TESPA) to prepare a novel adsorbent. The adsorption of methyl orange (MO) from aqueous solutions onto the modified wheat straw was studied. The adsorbent was characterized by scanning electron microscopy (SEM) and Fourier transform-infrared spectroscopy (FT-IR). FTIR results suggested that electrostatic interaction appears to be the principle mechanism of MO adsorption. The adsorption isotherm data were fitted to Langmuir, Sips and Redlich-Peterson equations, and the Langmuir adsorption capacity,  $Q_{\max}$ , reached  $304.2 \text{ mgg}^{-1}$ , while a  $Q_{\max}$  value of  $75.8 \text{ mgg}^{-1}$  was found for unmodified wheat straw. Also, it was observed that the adsorption of MO increases with increasing temperature from 303 to 323K, and the process is endothermic in nature. The removal of MO by TESP-ATWS followed pseudo-second order reaction kinetics based on Lagergren equations. Mechanism studies indicated that the adsorption of MO onto the TESP-ATWS was mainly governed by external mass transport, where particle diffusion was the rate limiting step.

**Keywords:** triethoxysilylpropylamine, modification, wheat straw, methyl orange, isotherm, kinetics

## INTRODUCTION

It is essential to remove dyes from industrial effluents as wastewater containing dye leads to serious environmental pollution.<sup>1</sup> Dyes are one of the most important classes of pollutants, and dye contaminated water is often difficult to treat, since they have a synthetic origin and a complex molecular structure, which makes them more stable and difficult to biodegrade.<sup>2</sup> The aromatic rings in their structure impart harmful features to them, such as carcinogenicity, inertia and mutagenicity.<sup>3</sup> The discharge of even small amounts of dye effluent into natural rivers can seriously affect the aquatic life, water bodies contaminated by synthetic dyes have already created serious environmental problems worldwide.<sup>4</sup>

Methyl orange (MO), an anionic dye, belongs to the azo group of dyes. The presence of the azo group (N=N) on MO and its low biodegradability

make it an issue of concern for environmental science.<sup>5</sup> Azo dyes are well-known carcinogenic organic substances. Like many other dyes of its class, MO can enter the body through inadvertent ingestion, and it can be metabolized into aromatic amines by intestinal microorganisms.<sup>6</sup>

In spite of the availability of many methods for wastewater treatment, such as adsorption, coagulation, chemical oxidation, membrane separation process, electrochemical, aerobic and anaerobic microbial degradation, most of them have not been very successful, because of their numerous limitations. Among them, adsorption is preferred due to its cheapness and the high quality of the treated effluents, especially for well-designed sorption processes.<sup>7</sup>

The removal of dyes and pigments from aqueous solutions *via* adsorption processes is a simple method known to be relatively low cost,

and such effective technology has been widely adopted by water treatment plants. The removal efficiency of dyes *via* adsorption mainly depends on the choice of the adsorbents employed.<sup>8</sup> Thus, the production of cheaper adsorbents to replace costly wastewater treatment methods, such as chemical precipitation, ion-exchange, electroflotation, membrane separation, reverse osmosis, electrodialysis, solvent extraction *etc.*, has attracted great research attention in recent years.<sup>9,10</sup>

Wheat straw, as a type of renewable crop wastes, is not only abundantly available, but also rich in reactive groups existing in cellulose, hemicelluloses and lignin structures. A promising way to valorize this precious bioresource is to turn it into an adsorbent. Although the adsorption capacity of raw straw is unsatisfactory, various chemical modifications, by introducing some functional groups, can be applied to improve it.<sup>11</sup> Alkali treatment is one of the widely employed chemical treatment techniques for surface modification of agricultural wastes for the purpose of improving their adsorption properties. The treatment of agricultural wastes with aqueous sodium hydroxide (NaOH) solutions breaks the covalent association between lignocellulose components, hydrolyzing hemicelluloses and depolymerizing lignin.<sup>2,12</sup> This treatment has a substantial influence on the morphological, molecular and supramolecular properties of cellulose, causing changes in crystallinity, pore structure, accessibility, stiffness, unit cell structure and orientation of fibrils in the cellulosic fibres.<sup>13,14</sup> NaOH also improves the mechanical and chemical properties of cellulose, such as structural durability, reactivity and natural ion-exchange capacity. The treatment with NaOH removes natural fats and waxes from the cellulose fiber surfaces, thus revealing chemically reactive functional groups, such as  $-OH$ .<sup>14,15</sup> Wheat straw has a vascular bundle structure, which will

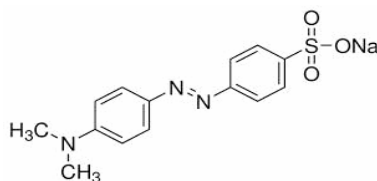
provide additional surface for chemical modification. It also has complicated components, such as pectin, protein and fatty acid, in addition to its major ones (lignin, hemicelluloses, cellulose), besides, it abounds in hydroxyl groups.<sup>7,16</sup>

Our literature survey revealed several reports on chemical modification of wheat straw by cetyltrimethyl ammonium bromide (CTAB),<sup>17</sup> ethylenediamine,<sup>18</sup> hexadecylpyridiniumbromide,<sup>19</sup> CPB and acrylic acid, acrylic amide and dimethyl diallyl ammonium chloride.<sup>20</sup> To the best of our knowledge, the application of triethoxysilylpropylamine (TESPA) coated alkali treated wheat straw (ATWS) for methyl orange (MO) removal from aqueous environment has not been reported so far. The aim of this study has been to investigate an efficient methodology to face the current challenges of color treatment of industrial textile wastewater effluents, using a chemically designed adsorbent based on wheat straw modified by triethoxysilylpropylamine (TESPA), for the adsorptive removal of methyl orange (MO) as an example of anionic dyes. The optimization of all the experimental controlling factors and conditions, such as reaction time, pH, adsorbent dosage, initial dye concentration, mechanism of adsorption and temperature, was also explored.

## EXPERIMENTAL

### Materials

Wheat straw (WS) was obtained from a local wheat field in Ardebil, Iran. Before grinding, the raw material was cleaned and dried at 378 K for 24 h. The dried wheat straw was then ground and sieved to a size range of 100-500  $\mu\text{m}$ . Finally, the resulting product was stored in an air-tight container for further use. The chemical composition of the wheat straw was determined as follows: 43.1% cellulose (Kurshchner), 19.31% lignin, 72.12% holocellulose, 6.8% ash and 1.64% ethanol/dichloromethane extractables, on an oven-dry weight basis (moisture content of 7.8%).



Scheme 1: Molecular structure of methyl orange

Methyl orange (MO) (Merck, No. 101322) was selected as an anionic dye. Scheme 1 shows the molecular structure of MO. Triethoxysilylpropylamine (TESPA) (Merck, No. 821619) was used for chemical modification of wheat straw. A stock solution of MO was prepared by dissolving 1.0 g of MO in 1 L of deionized water, and the concentrations of MO used (50-500 mg/L) were obtained by dilution of the stock solution. The pH of the solution was adjusted to the desired value by adding a small quantity of 0.01 mol/L HCl or 0.01 mol/L NaOH.

#### Preparation of alkali-treated wheat straw (ATWS)

Raw wheat straw (RWS) was prepared as described previously. The dried RWS was treated in a 0.06 M sodium hydroxide (NaOH) solution for 4 h at room temperature. The sample was then washed thoroughly with distilled water until the sample was neutralized and dried in the oven at 333 K for 24 h. Finally, the resulting adsorbent, alkali-treated wheat straw (ATWS), was stored in an air-tight container until further use in adsorption experiments.

#### Modification of ATWS by TESPA

In a typical reaction, 30 mL of TESPA was added dropwise to a suspension of 15 g ATWS in 200 mL dry toluene. The mixture was stirred at room temperature for 30 min. The residue material was separated by filtration, washed with dichloromethane and dried at 333 K for 24 h. This sample was denoted TESPA-ATWS. Dichloromethane (Merck, No. 1.06050) and toluene (Merck, No. 108-88-3) were used as solvents for the modification reaction.

#### Characterization

Fourier transform infrared (FTIR) analysis was applied to determine the surface functional groups, using an FTIR spectroscope (FTIR-2000, Bruker), where the spectra were recorded from 3500 to 500  $\text{cm}^{-1}$ . Surface morphology was studied using scanning electron microscopy (Vegall-Tescan Company).

#### Point of zero charge ( $\text{pH}_{\text{pzc}}$ ) determination

In point of zero charge ( $\text{pH}_{\text{pzc}}$ ) determination, 0.01 M NaCl was prepared and its pH was adjusted in the range of 2-11 by adding 0.01 M NaOH or HCl. Then, 50 mL of 0.01 M NaCl was put in a conical flask and then 0.1 g of TESPA-ATWS was added to the solution. The flasks were kept for 72 h and the final pH of the solution was measured using a pH meter.

#### Batch adsorption experiments

Equilibrium studies were carried out by contacting a fixed amount of TESPA-ATWS (0.2 g) with 100 mL of MO solution with different initial concentrations (50, 100, 200, 300, 400 and 500 mg/L) in 250 mL stopper Erlenmeyer flasks at a temperature of 303 K

and pH 2. The procedure was repeated for temperatures of 313 and 323 K. MO concentrations were determined by spectrometry at the wavelength of maximum absorbance, 492 nm, using a double beam UV-Vis spectrophotometer (Shimadzu, Model UV 2100, Japan).

The adsorption capacity ( $q_e$ ) was calculated according to Equation 1:

$$q_e = (C_0 - C_e)V/W \quad (1)$$

where  $C_0$  (mg/L) and  $C_e$  (mg/L) are the initial and the final or equilibrium MO concentration, respectively.  $V$  (mL) is the volume of the MO solution, and  $W$  is the mass (g) of the dry adsorbent (TESPA-ATWS) used.

#### Kinetic studies

Adsorption kinetics experiments were performed by contacting 200 mL MO solution of different initial concentrations ranging from 50 to 200 mg/L with 0.4 g TESPA-ATWS in a 250 mL stopper red conical flask at room temperature. At fixed time intervals, the samples were taken from the solution and were analyzed by spectrometry at the wavelength of maximum absorbance, 492 nm.

#### Isotherm modeling

The non-linear forms of the Langmuir, Freundlich, Temkin, Sips and Redlich-Peterson isotherm models were used to analyze the equilibrium isotherm data.<sup>7,21</sup> The fitness of these models was evaluated by the non-linear coefficients of determination ( $R^2$ ). The Matlab (version 7.3) software package was used for the computing.

The Langmuir adsorption isotherm assumes that adsorption takes place at specific homogeneous sites within the adsorbent and has found successful application for many processes of monolayer adsorption.<sup>22</sup> The Freundlich isotherm is derived by assuming a heterogeneous surface with a non-uniform distribution of sorption heat over the surface.<sup>23</sup> The Sips model is an additional empirical model that has the features of both the Langmuir and Freundlich isotherm models. As a combination of the Langmuir and Freundlich isotherm models, the Sips model contains three parameters,  $Q_{\text{max}}$ ,  $K_s$  and  $1/n$ , which can be evaluated by fitting the experimental data.<sup>24</sup>

Similar to the Sips isotherm, Redlich and Peterson proposed an isotherm comprising the features of the Langmuir and the Freundlich isotherms. The Temkin isotherm was first developed by Temkin and Pyzhev, and it is based on the assumption that the heat of adsorption would decrease linearly with the increase of coverage of adsorbent. The Temkin isotherm equation was applied to describe adsorption on heterogeneous surfaces.<sup>2</sup>

### Kinetic models

The Lagergren rate equation<sup>25</sup> is one of the most widely used adsorption rate equations for the adsorption of a solute from a liquid solution. In this work, we used the linear form of the pseudo-first order and pseudo-second order kinetic models.

### Statistical analysis

All experiments were performed in duplicate and the mean values were presented. The data were analyzed by one-way analysis of variance (ANOVA), using SPSS 11.5 for Windows. The data were considered statistically different from the control at  $P < 0.05$ .

## RESULTS AND DISCUSSION

### Characterization of TESP-ATWS

#### FTIR analysis

Figure 1 shows the FTIR spectra of WS, ATWS, TESP-ATWS before and after MO adsorption, respectively. In Figure 1a and b, the broad peak around  $3440\text{ cm}^{-1}$  is the characteristic peak of WS, corresponding to bonded hydroxyl groups of cellulose and lignin.<sup>26</sup> The strong C–O–

C band at around  $1044\text{ cm}^{-1}$  also confirms the cellulose and lignin structures. The weak band at  $2890\text{ cm}^{-1}$  was assigned to the stretch vibration of C–H bond in methylene groups.<sup>27</sup> The peak at  $1625\text{ cm}^{-1}$  in Figure 1c is due to the bending frequency of the amino group of TESP anchored to the chain backbone.<sup>28</sup> This band shifts to lower frequency,  $1682\text{ cm}^{-1}$ , in TESP-ATWS after MO adsorption (Fig. 1d). In the FTIR spectrum of MO, –C=C– stretching is observed at  $1599\text{ cm}^{-1}$ , –S=O stretching at  $1120\text{ cm}^{-1}$ , –C=N stretching at  $1314\text{ cm}^{-1}$ , and –N–H stretching at  $3209\text{ cm}^{-1}$ .<sup>29</sup>

In this work, the –S=O stretching vibration band ( $1120\text{ cm}^{-1}$ ) shifts to lower frequency,  $1182\text{ cm}^{-1}$ , in the spectrum of TESP-ATWS after MO adsorption (Fig. 1d). These observations clearly provide evidence that ATWS was modified by TESP and MO was anchored to TESP-ATWS. Scheme 2 shows our proposed mechanism for modification of wheat straw by triethoxysilylpropylamine and MO adsorption on TESP-ATWS.

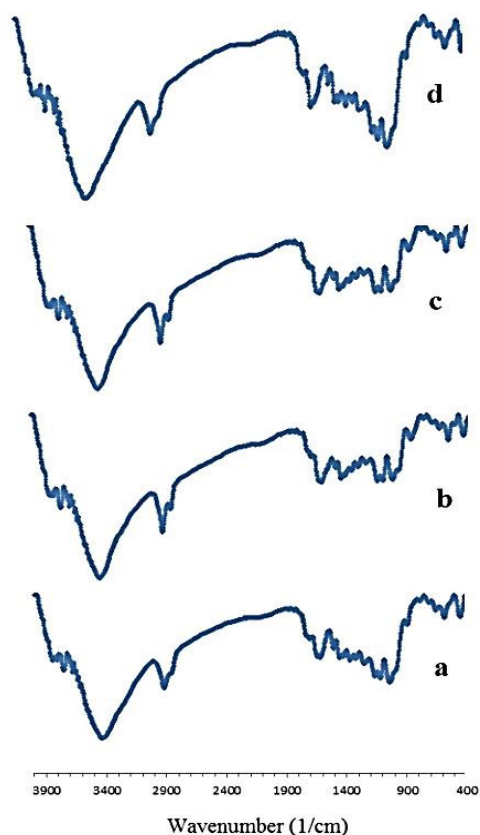
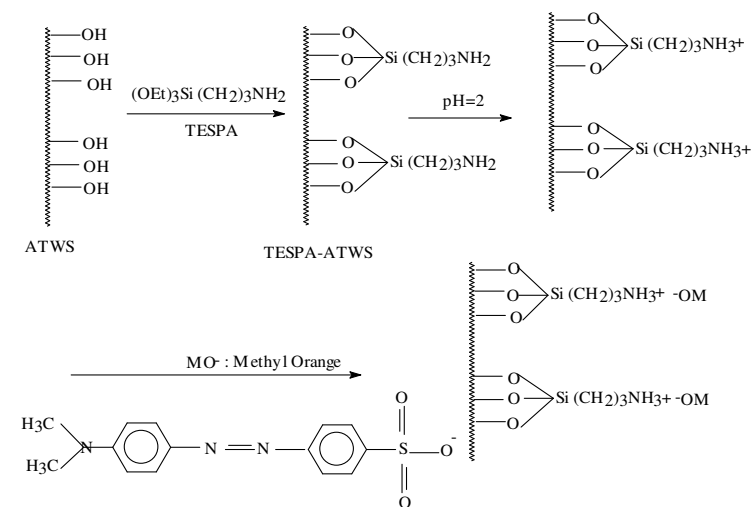


Figure 1: FTIR spectra of a) WS, b) ATWS and TESP-ATWS c) before and d) after MO adsorption



Scheme 2: Our proposed mechanism for MO adsorption on TESPA-ATWS

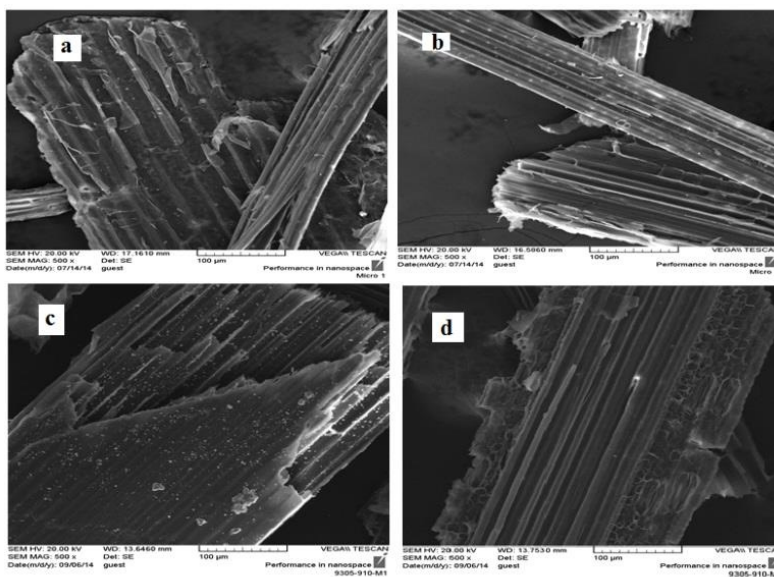


Figure 2: SEM micrographs of a) WS, b) ATWS and TESPA-ATWS c) before and d) after MO adsorption

### SEM analysis

The surface morphologies of WS, ATWS, TESPA-ATWS before and after MO adsorption were observed, as shown in Figure 2. It was found that the irregular superficial layer of protective silica and natural resins on WS (Fig. 2a) were removed after the alkali treatment,<sup>30</sup> which was beneficial to the modification in the following step. In addition, after modification by triethoxysilylpropylamine, the surface of wheat straw became rough, which increased the specific area of the adsorbent and contributed to enhancing the adsorption capacity.

### Study of MO adsorption

#### *Point of zero charge ( $\text{pH}_{\text{pzc}}$ ) studies and the effect of pH on MO adsorption*

The linear range of pH sensitivity, the type of surface active centers and the adsorption ability of the surface can be determined by the point of zero charge ( $\text{pH}_{\text{pzc}}$ ) factor.<sup>31</sup> Many researchers studied the point of zero charge of adsorbents prepared from agricultural solid wastes in order to better understand their adsorption mechanism.<sup>32</sup> Cationic dye adsorption is favored at  $\text{pH} > \text{pH}_{\text{pzc}}$ , due to the presence of functional groups, such as  $\text{OH}^-$  and  $\text{COO}^-$  groups. Anionic dye adsorption is

avored at  $\text{pH} < \text{pH}_{\text{pzc}}$ , where the surface becomes positively charged.<sup>33</sup>

Figure 3 shows the graph of  $\text{pH}_{\text{final}}$  vs  $\text{pH}_{\text{initial}}$  in this work. The intersections of the curves with the straight line are known as the end points of the  $\text{pH}_{\text{pzc}}$ , and this value is 3 for TESPА-ATWS. Figure 4 shows the effect of pH on the adsorption of MO. The experiments were conducted at 100 mL of 100 mg/L initial MO concentration and 0.20 g TESPА-ATWS dose. It was observed that pH has a significant influence to the adsorption process. MO is an anionic dye, which exists in aqueous solution in the form of negatively charged ions. As a charged species, the degree of its adsorption onto the adsorbent surface is primarily influenced by the surface charge on the adsorbent, which in turn is influenced by the solution pH. As shown in Figure 4, the equilibrium concentration ( $q_e$ ) was maximum at pH 2 (48 mg/g). Higher adsorption of MO at acidic pH ( $\text{pH} < \text{pH}_{\text{pzc}}$ ) is due to the presence of excess  $\text{H}^+$  ions, and the adsorption of positively

charged dye anions is enhanced through electrostatic forces of attraction. At higher solution pH ( $\text{pH} > \text{pH}_{\text{pzc}}$ ), it is possible that negatively charged hydroxyl anions ( $\text{OH}^-$ ) compete with the anionic groups on the dye for adsorption sites. We selected  $\text{pH}=2$  for adsorption and kinetic experiments.

#### Effect of adsorbent dosage

Adsorbent dosage is an important parameter that strongly influences the adsorption process by affecting the adsorption capacity.<sup>34</sup> Therefore, the influence of adsorbent dosage on MO adsorption by TESPА-ATWS was investigated in the range of 0.01-0.3 g (Fig. 5). The adsorption efficiency increased from 34% to 99% as the adsorbent dosage was increased from 0.01 to 0.2 g. The increase in the percentage of MO removal with increasing adsorbent dosage could be attributed to an increase in the adsorbent surface area, augmenting the number of adsorption sites available for adsorption, as already reported.<sup>35</sup>

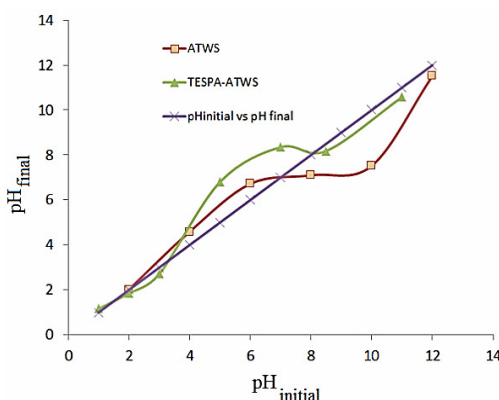


Figure 3: Plot for determination of point of zero charge pH of TESPА-ATWS

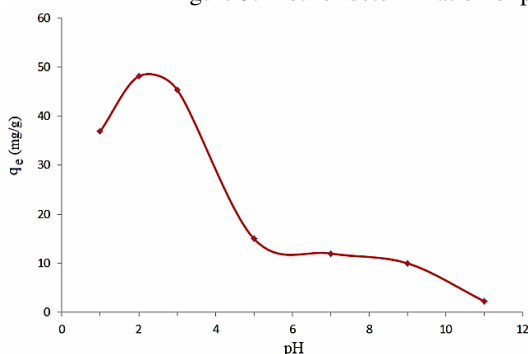


Figure 4: Effect of solution pH on adsorption of MO on TESPА-ATWS

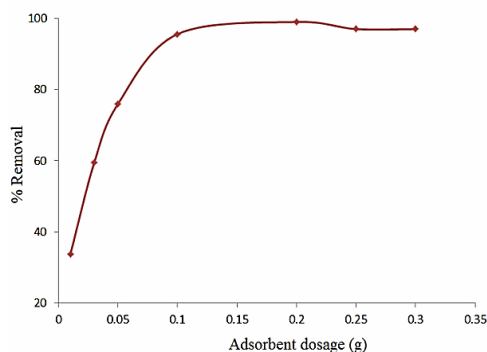


Figure 5: Effect of adsorbent dosage on adsorption of MO

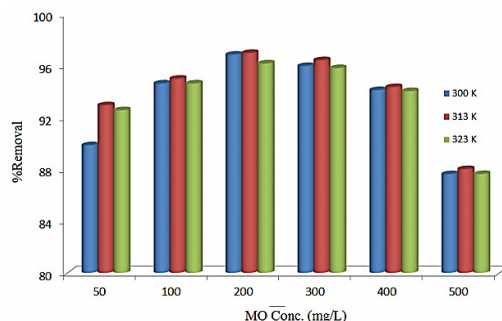


Figure 6: Effect of temperature on removal of MO at different initial concentrations

Table 1  
Isotherm parameters for MO adsorption by TESP-ATWS

Isotherm		Temperature (K)	303	313	323
Langmuir	$q_e = q_m K_a C_e / (1 + K_a C_e)$	$Q_{max}$ (mg/g)	250.1	304.2	273.1
		$k_L$ (L/mg)	0.0985	0.0762	0.0521
		$R^2$	0.9998	0.9941	0.9952
Freundlich	$q_e = K_F C_e^{1/n}$	$n$	2.290	2.199	1.971
		$k_F$ (dm <sup>3</sup> /mg) <sup>1/n</sup>	40.01	38.35	30.62
		$R^2$	0.9605	0.9788	0.9623
Temkin	$q_e = RT/B(\ln k_T C_e)$	$B/RT$	0.0198	0.0222	0.0158
		$k_T$ (L/mg)	1.229	1.785	0.5936
		$R^2$	0.9923	0.9318	0.9882
Sips	$q = \frac{q_m b C_e^{1/n}}{1 + b C_e^{1/n}}$	$Q_{max}$ (mgg <sup>-1</sup> )	247.1	308.5	273.3
		$K_s$ ((mg <sup>-1</sup> ) <sup>1/n</sup> )	0.097	0.0837	0.0441
		$1/n$	1.020	0.860	1.152
		$R^2$	0.9999	0.9952	0.9993
Redlich-Peterson	$q = \frac{a C_e}{1 + b C_e^n}$	$K_{rp}$ (LKg <sup>-1</sup> )	24.48	23.46	14.74
		$\alpha_{rp}$ (Kgmg <sup>-1</sup> )	0.09621	0.1195	0.03462
		$\beta$	1.004	0.9207	1.079
		$R^2$	0.9998	0.9944	0.9956

### Effect of temperature on MO adsorption

Figure 6 shows the effect of temperature on the adsorption rate of MO onto TESP-ATWS, investigated at three different temperatures (300, 313 and 323 K), using the initial concentration of 50-500 mg/L. It is observed that the removal percentage of MO increases with increasing temperature at all concentrations studied. An increase in temperature increases the rate of diffusion of the adsorbate molecules across the external boundary layer and within the internal pores of the adsorbent particles, due to a decrease in the viscosity of the solution.<sup>38</sup> The obtained results revealed that an increase in temperature from 300 to 313 K increased the TESP-ATWS monolayer adsorption capacity from 250.1 to 304.2 mg/g (Table 1). This phenomenon indicates that the adsorption process is endothermic in nature.<sup>2</sup> This may be due to the mobility of

molecules, which increases generally with a rise in temperature, thereby facilitating the formation of surface monolayers.<sup>39</sup>

### Effect of initial concentration and contact time on MO adsorption

Figure 7 shows the effect of the initial dye concentration (50-200 mg/L) on the adsorption of MO. It was observed that the amount of MO adsorbed was rapid during the first 10 min and thereafter it proceeded at a slower rate (10-100 min), until saturation was finally reached. The equilibrium adsorption increases with an increase in the initial MO concentration from 50 to 200 mg/L. The findings are explained by the fact that, as the initial concentration increases, the mass transfer driving force becomes larger, hence resulting in higher MO adsorption.<sup>40</sup> Also, Figure 7 highlights that the contact time needed for MO

solutions with initial concentrations of 50-200 mg/L to reach equilibrium was 100 min. The initial concentration provides an important driving force to overcome all mass transfer resistances of the MO between the aqueous and solid phase. However, the experimental data were measured at 120 min to be sure that full equilibrium was attained.

#### Adsorption equilibrium isotherm

Isotherm data analysis is important to develop equations that correctly represent the results and could be used for design purposes. Figure 8 and Table 1 show the fitting parameters for the measured isotherm data for MO adsorption onto TESPATWS on the non-linear forms of the Langmuir, Freundlich, Temkin, Sips and Redlich-Peterson models. The values of  $R^2$  for the

Langmuir, Sips and Redlich-Peterson isotherm models indicate a good fit with the three models. The applicability of the Langmuir, Sips and Redlich-Peterson isotherms shows that there was effective monolayer sorption and a homogeneous distribution of active sites on the surface of TESPATWS. Among all the isotherm equations, at all the temperatures, the Freundlich isotherm presented the poorest fit to the experimental data. The value of exponent  $1/n$  for the Sips model is close to unity, indicating that adsorptions are quite homogeneous. The monolayer capacity ( $Q_{max}$ ) is  $304.2 \text{ mg g}^{-1}$ , as calculated from the Langmuir isotherm at 313 K (Table 1). Also, there is similarity between  $Q_{max}$  values obtained from the Langmuir and Sips models at all the temperatures.

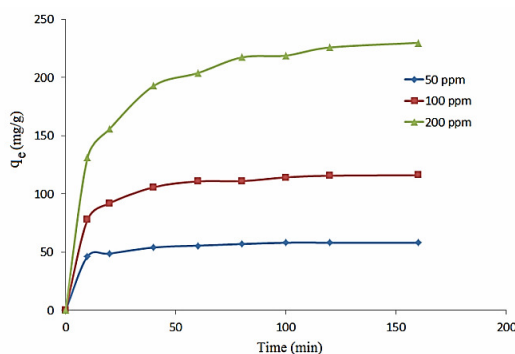


Figure 7: Effect of contact time and initial concentration on the adsorption of MO on TESPATWS

#### Kinetics of adsorption

The dynamics of the adsorption can be studied by the kinetics of adsorption in terms of the order of the rate constant.<sup>41,42</sup> The adsorption rate is an important factor for a better choice of the material to be used as an adsorbent; the adsorbent should have a high adsorption capacity and a fast adsorption rate.<sup>2</sup> Most adsorption studies use pseudo-first-order and pseudo-second-order models to study the adsorption kinetics. For the pseudo-first-order model, the adsorption rate was expected to be proportional to the first power of concentration, where the adsorption was characterized by diffusion through a boundary. The pseudo-first-order model sometimes does not fit well for the whole range of contact time, when it fails theoretically to predict the amount of dye adsorbed and thus deviates from the theory. In this case, the pseudo-second-order equation used was based on the sorption capacity of the solid phase, where the pseudo-second-order model assumes that chemisorption may be the rate-

controlling step in the adsorption processes.<sup>43,44</sup> The transient behavior of the MO adsorption process was analyzed by using the pseudo-first and pseudo-second-order kinetic models. Plotting  $\ln(q_e - q_t)$  against  $t$  permits the calculation of  $k_1$  (Fig. 9a). The rate constant,  $k_1$ , evaluated from these plots with the correlation coefficients obtained are listed in Table 2. Plotting  $t/q$  against  $t$  (Fig. 9b) gives a straight line, where  $k_2$  can be calculated. Usually, the best-fit model can be selected based on the linear regression correlation coefficient  $R^2$  values. Generally, the kinetic adsorption is better represented by the pseudo-second-order model for anionic and cationic dye adsorption.

The  $R^2$  values listed (in Table 2) for the pseudo-first-order kinetic model were between 0.956 and 0.980. The  $R^2$  value for the pseudo-second-order model was 0.999, which is higher than the  $R^2$  values obtained for the pseudo-first-order model. Therefore, the adsorption kinetics could be more favorably described by the pseudo-

second-order kinetic model for MO adsorption

onto TESPA-ATWS.

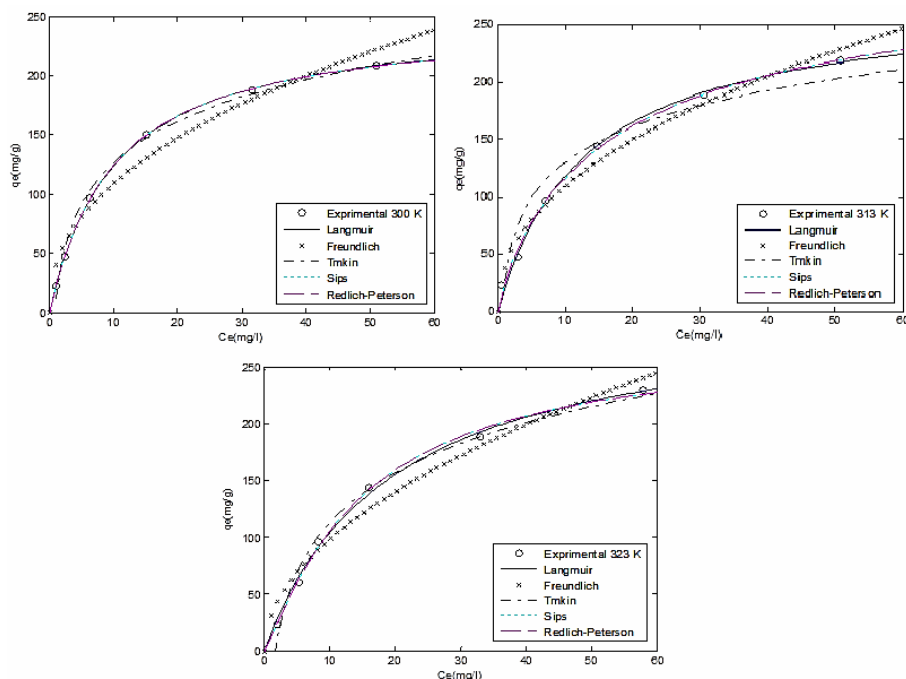


Figure 8: Isotherm plots for MO adsorption onto TESPA-ATWS at different temperatures

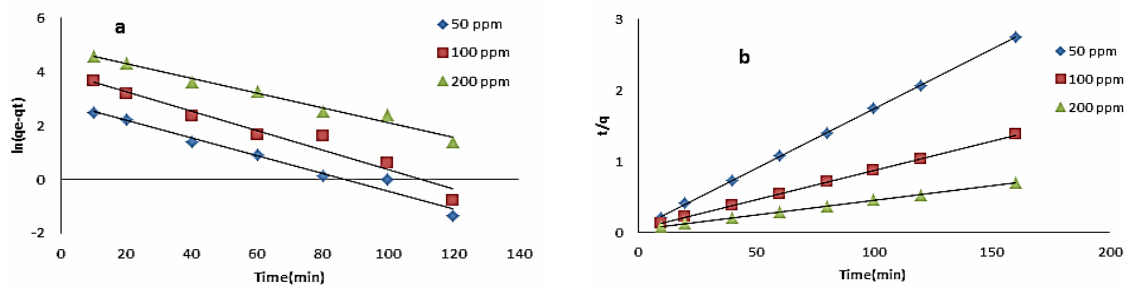


Figure 9: Kinetic models for adsorption of MO onto TESPA-ATWS; (a) pseudo-first-order and (b) pseudo-second-order rate equations

### Adsorption mechanism of MO

It is now well established that, during the adsorption of dye onto a porous adsorbent, the following three consecutive steps take place:<sup>45,46</sup>

- (i) Transport of the ingoing adsorbate ions to the external surface of the adsorbent (film diffusion);
- (ii) Transport of the adsorbate ions within the pores of the adsorbent, except for a small amount of adsorption, which occurs on the external surface (particle diffusion);
- (iii) Adsorption of the ingoing adsorbate ions onto the interior surface of the adsorbent.<sup>45</sup>

Out of these three processes, the third process is considered to be very fast and is not the rate

limiting step in the uptake of organic compounds. The remaining two steps impart the following three possibilities:

Case 1: External transport > internal transport, where the rate is governed by particle diffusion.

Case 2: External transport < internal transport, where the rate is governed by film diffusion.

Case 3: External transport  $\approx$  internal transport, which accounts for the transport of the adsorbate ions to the boundary and may not be possible within a significant rate, which later on gives rise to the formation of a liquid film surrounded by the adsorbent particles with a proper concentration gradient.

Table 2  
Kinetic parameters for adsorption of MO onto TESPА-ATWS based on Lagergren rate equation

Kinetic model	Equation	Linear form	$C_0$	$R^2$	$k_1$	$q_e$
			(mg/L)		(1/min)	(mg/g)
Pseudo-first order	$dq/q_e - q = k_1 dt$	$\ln(q_e - q_t) = \ln q_e - k_1 t$	50	0.974	0.032	58.079
			100	0.956	0.036	116.026
			200	0.980	0.027	229.684
			$C_0$	$R^2$	$k_2$	$q_e$
			(mg/L)		(mg/g.min)	(mg/g)
Pseudo-second order	$dq/(q_e - q_t)^2 = k_2 dt$	$1/(q_e - q_t) - 1/q_e = k_2 t$	50	0.999	0.0041	62.5
			100	0.999	0.0012	125
			200	0.999	0.0004	250

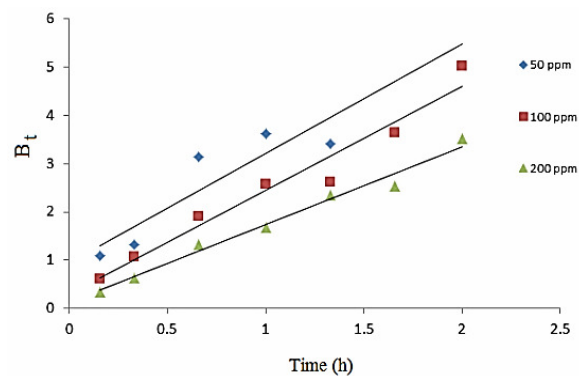


Figure 10: Plot of  $B_t$  vs time for different initial concentrations of MO

In order to predict the actual slow step involved in the adsorption process, the kinetic data were further analyzed using the Boyd model given by Equation 2:<sup>47</sup>

$$B_t = -0.4977 - \ln(1-F) \quad (2)$$

where F represents the fraction of solute adsorbed at any time, t (h), as calculated using Equation 3:

$$F = q_t/q_e \quad (3)$$

where  $q_t$  and  $q_e$  are amounts adsorbed after time t and after infinite time (160 min), respectively. The calculated  $B_t$  values were plotted against time t (h), as shown in Figure 9.

The plot of  $B_t$  vs time distinguishes between the film-diffusion and particle-diffusion-controlled rates of adsorption. The linear lines for all MO initial concentrations did not pass through the origin and the points were scattered. This indicated that the adsorption of MO onto the TESP-ATWS was mainly governed by external mass transport, where particle diffusion was the rate limiting step.<sup>47</sup>

#### Desorption studies of MO

Desorption studies can provide an insight into the mechanism of an adsorption process. If the dye adsorbed onto the adsorbent can be desorbed by water, it can be concluded that the adsorption occurred by weak bonds. If strong acids, such as HCl, can desorb the dye, it can be said that the attachment of the dye onto the adsorbent is by ion exchange.<sup>48</sup> Hence, neutral distilled water was used in the elution of MO molecules from the TESP-ATWS, followed by HCl solution. The percentage of desorption obtained was 2 and 10%, when using neutral distilled water and 0.1 M HCl solution, respectively. The fact that low desorption occurred with distilled water and much higher desorption with the HCl solution suggests that the adsorption of MO onto TESP-ATWS was carried out significantly by ion exchange. As presented in Scheme 2, the MO dye was adsorbed onto the TESP-ATWS surface through strong electrostatic interaction.

#### CONCLUSION

The current study demonstrates that wheat straw modified by triethoxysilylpropylamine can be used effectively for adsorption of methyl orange (MO) dye from aqueous solutions. The adsorption of MO onto TESP-ATWS strongly depended on the solution pH level, initial MO concentration and temperature. Non-linear isotherm analyses indicated that the equilibrium isotherm data are

best described by the Langmuir model. The adsorption capacity was found to be 304.2 mgg<sup>-1</sup> at 313 K. We obtained a Langmuir adsorption capacity,  $Q_{max}$ , of 75.8 mgg<sup>-1</sup> for unmodified wheat straw. MO adsorption follows pseudo-second order kinetics, which obeys the monolayer chemical adsorption mechanism.

**ACKNOWLEDGMENTS:** The authors wish to acknowledge the financial support of the University of Tehran.

#### REFERENCES

- <sup>1</sup> B. Zhao, W. Xiao, Y. Shang, H. Zhu and R. Han, *Arabian J. Chem.*, **10**, S3595 (2017).
- <sup>2</sup> A. Ebrahimian Pirbazari, E. Saberikhah, M. Badrouh and M. S. Emami, *Water Resources and Industry*, **6**, 64 (2014).
- <sup>3</sup> Y. Su, Y. Jiao, C. Dou and R. Han, *Desalin. Water Treat.*, **52**, 6145 (2013).
- <sup>4</sup> A. Ebrahimian and E. Saberikhah, *Cellulose Chem. Technol.*, **47**, 657 (2013).
- <sup>5</sup> E. Bazrafshan, A. A. Zarei, H. Nadi and M. A. Zazouli, *Indian J. Chem. Technol.*, **21**, 105 (2014).
- <sup>6</sup> P. Pookmanee, S. Angkana and S. Phanichphant, *Adv. Mater. Res.*, **93-94**, 320 (2010).
- <sup>7</sup> A. Ebrahimian Pirbazari, E. Saberikhah and S. S. Habibzadeh Kozani, *Water Resources and Industry*, **6**, 23 (2014).
- <sup>8</sup> R. K. Xu, S. C. Xiao, J. H. Yuan and A. Z. Zhao, *Bioresour. Technol.*, **102**, 10293 (2011).
- <sup>9</sup> W. S. Wan Ngah and M. A. Hanafiah, *Bioresour. Technol.*, **99**, 3935 (2008).
- <sup>10</sup> C. Deepika, S. Dipak and P. Anjani, *Eur. Chem. Bull.*, **2**, 880 (2013).
- <sup>11</sup> W. Zhang, H. Li, X. Kan, L. Dong, H. Yan *et al.*, *Bioresour. Technol.*, **117**, 40 (2012).
- <sup>12</sup> J. Vadiveloo, B. Nurfariza and J. G. Fadel, *Anim. Feed Sci. Technol.*, **151**, 299 (2009).
- <sup>13</sup> J. Siroky, R. S. Blackburn, T. Bechtold, J. Taylor and P. White, *Carbohydr. Polym.*, **84**, 299 (2011).
- <sup>14</sup> J. F. Castañón-Rodríguez, J. Welti-Chanes, A. J. Palacios, B. Torrestiana Sanchez, J. A. Ramírez de León *et al.*, *CyTA – J. Food*, **13**, 613 (2015).
- <sup>15</sup> B. S. Ndazi, S. Karlsson, J. V. Tesha and C. W. Nyahumwa, *Composites Part A*, **38**, 925 (2007).
- <sup>16</sup> Y. Tian, M. Wu, X. Lin, P. Huang and Y. Huang, *J. Hazard. Mater.*, **193**, 10 (2011).
- <sup>17</sup> R. Zhang, J. Zhang, X. Zhang, C. Dou and R. Han, *J. Taiwan Inst. Chem. Eng.*, **45**, 2578 (2014).
- <sup>18</sup> Z. Wang, P. Han, Y. Jiao, D. Ma, C. Dou *et al.*, *Desalin. Water Treat.*, **30**, 195 (2011).
- <sup>19</sup> Y. Su, B. L. Zhao, W. Xiao and R. P. Han, *Environ. Sci. Pollut. Res.*, **20**, 2058 (2013).
- <sup>20</sup> Z. Ma, Q. Li, Q. Yue, B. Gao, X. Xu *et al.*, *Bioresour. Technol.*, **102**, 2853 (2011).
- <sup>21</sup> Y. Liu and Y. J. Liu, *Sep. Purif. Technol.*, **61**, 229 (2008).

- <sup>22</sup> M. E. Ossman and M. S. Mansour, *Int. J. Ind. Chem.*, **4**, 13 (2013).
- <sup>23</sup> N. Mosallanejad and A. Arami, *J. Chem. Health Risks*, **2**, 31 (2012).
- <sup>24</sup> A. Ebrahimián, E. Saberikhah, M. S. Emami and M. Sotudeh, *Cellulose Chem. Technol.*, **48**, 735 (2014).
- <sup>25</sup> S. Lagergren and K. Sven, *Vetenskapsakad. Handl.*, **24**, 1 (1898).
- <sup>26</sup> R. Bodírlău, C. A. Teacă and I. Spiridon, *Bioresources*, **4**, 1285 (2009).
- <sup>27</sup> Y. Su, B. Zhao, W. Xiao and R. Han, *Environ. Sci. Pollut. Res.*, **20**, 5558 (2013).
- <sup>28</sup> A. Ebrahimián and M. A. Zanjanchi, *Korean J. Chem. Eng.*, **31**, 218 (2014).
- <sup>29</sup> R. Nandini and B. Vishalakshi, *E-J. Chem.*, **9**, 1 (2012).
- <sup>30</sup> C. G. Rocha, D. A. M. Zaia, R. V. D. Alfaya and A. A. D. Alfaya, *J. Hazard. Mater.*, **166**, 383 (2009).
- <sup>31</sup> A. Poghossian, *Chemistry*, **44**, 155 (1997).
- <sup>32</sup> M. T. Yagub, T. K. Sen, S. Afroze and H. M. Ang, *Adv. Colloid Interface Sci.*, **209**, 172 (2014).
- <sup>33</sup> M. A. M. Salleh, D. K. Mahmoud, W. A. W. A. Karim and A. Idris, *Desalination*, **280**, 1 (2011).
- <sup>34</sup> S. N. A. Abas, M. H. S. Ismail, Md. L. Kamal and S. Izhar, *World Appl. Sci.*, **28**, 1518 (2013).
- <sup>35</sup> M. R. Fathi, A. Asfaram, A. Hadipour and M. Roosta, *J. Environ. Health Sci. Eng.*, **12**, 1 (2014).
- <sup>36</sup> E. A. Ashour, M. A. Tony and P. J. Purcell, *Am. J. Chem. Eng.*, **2**, 92 (2014).
- <sup>37</sup> Ö. Dülger, F. Turak, K. Turhan and M. Özgür, *ISRN Anal. Chem.*, **2013**, article ID 210470 (2013).
- <sup>38</sup> J. Ghasemi and S. Asadpour, *J. Chem. Thermodyn.*, **39**, 967 (2007).
- <sup>39</sup> Y. Bulut and H. Karaer, *J. Dispersion. Sci. Technol.*, **36**, 61 (2015).
- <sup>40</sup> K. Belay and A. Hayelom, *Chem. Mater. Res.*, **6**, 31 (2014).
- <sup>41</sup> H. Z. Mousavi and Z. Lotf, *Int. J. Appl. Chem.*, **7**, 49 (2012).
- <sup>42</sup> V. Gómez, M. S. Larrechi and M. P. Callao, *Chemosphere*, **69**, 1151 (2007).
- <sup>43</sup> G. Crini and P. M. Badot, *Progress Polym. Sci.*, **33**, 399 (2008).
- <sup>44</sup> Z. Aksu, *Process Biochem.*, **40**, 997 (2005).
- <sup>45</sup> S. Karthikeyan, B. Sivakumar and N. Sivakumar, *E-J. Chem.*, **7**, S175 (2010).
- <sup>46</sup> W. J. Weber and J. C. Morris, *J. Sanit. Eng. Div.*, **89**, 31 (1963).
- <sup>47</sup> A. W. Tan and B. H. Hameed, *J. Appl. Sci.*, **10**, 2565 (2010).
- <sup>48</sup> D. Mall, V. C. Srivastava, G. V. A. Kumar and I. M. Mishra, *Colloids Surf., A: Physicochem. Eng. Aspects*, **278**, 175 (2006).